Supporting Information

Solution Structures of Chemoenzymatically Synthesized Heparin and its Precursors

Zhenqing Zhang, Scott A. McCallum, Jin Xie, Lidia Nieto, Francisco Corzana, Jesús Jiménez-Barbero, Miao Chen, Jian Liu, Robert J. Linhardt

Methods

Preparation of [^{13}C, ^{15}N]*N*-acetylheparosan. ^{13}C,^{15}N isotopically labeled *N*-acetylated heparosan (-GlcA(1,4)GlcNAc-) was prepared by fermentation of *E. coli* K5 strain (from American Type Culture Collection) in minimal media containing 2g/l of ^{13}C-D-glucose (Cambridge Isotope Laboratories) and 1 g/l of $^{15}NH_4Cl$ (Sigma, St. Louis, MO). The culture was incubated at 37 °C overnight. *N*-acetylheparosan was harvested from the medium of *E. coli* K5 culture following a procedure described by Vann and colleagues.[1] Briefly, the bacteria medium was diluted with equal volume of a buffer containing 20mM sodium acetated and 50 mM sodium chloride at pH 5.0. The resultant solution was then loaded onto a DEAE fast-flow (GE Healthcare, Amersham, Uppsala Sweden) column (1.5 × 20 cm) at a flow rate of 5 ml/min. ^{13}C,^{15}N labeled *N*-acetyheparosan was then eluted with 1 M sodium chloride in 20 mM sodium acetate (pH 5.0). We typically obtained 50 mg of heparosan from one liter of bacteria culture. The product was further purified by S200 HR Sephacryl (Sigma, St. Louis, MO) before it was subjected to NMR analysis.

Preparation of *N*-deacetylated heparosan. ^{13}C,^{15}N-labeled heparosan (5 mg) was dissolved in sodium hydroxide (50.0 ml, 2 M), incubated for 24 h at 60 °C, and cooled to room temperature, and was adjusted to pH 7 with concentrated hydrochloric acid. The reaction product was dialyzed against distilled water (MWCO 1000 Da) and lyophilized to obtain completely *N*-deacetylated heparosan intermediate with uniformly isotopic label. The uniformly isotopically labeled *N*-deacetylated heparosan intermediate (~5 mg in 1.2 ml distilled water) was treated with $NaHCO_3$ (25 mg) and $(CH_3)_3N{\bullet}SO_3$ complex (25 mg) in a single step and incubated at 50 °C for 12 h. Equal portion of $NaHCO_3$ and $(CH_3)_3N{\bullet}SO_3$ was added two more times at 12 h intervals. The solution was then brought to room temperature and dialyzed overnight against distilled water (MWCO 1000 Da). The dialyzate was lyophilized to obtain pure, completely *N*-substituted, ^{13}C,^{15}N-labeled *N*-sulfoheparosan (-GlcA(1,4)GlcNS-) (5 mg).

Enzymatic modification of *N*-sulfoheparosan. First, ^{13}C,^{15}N-labeled *N*-sulfoheparosan (~5 mg) was incubated at 37 °C with C_5-epimerase (17 mg) for 1 h in 50 mM MES (pH 7.0) containing 2 mM $CaCl_2$ in 10 ml. the solution was then mixed with immobilized 2-OST (100 mg, 95 units/μg, where 1 unit = 1 pmole sulfo group transferred/h), and components for the PAPS regeneration system including 40 μM PAP, 1 mM *p*-nitrophenol sulfate, and 0.4 mg/ml arylsulfotransferase IV (AST-IV) in the final volume of 40 ml. The mixture was incubated at 25 °C overnight with gentle shaking. The

supernatant was collected. The immobilized 2-OST was washed with 1 M sodium chloride in 25 mM Tris (pH 7.5) to elute any remaining polysaccharide products from the resin. The supernatant with the washes were combined, and the concentration of the sodium was reduced to lower than 250 mM. The polysaccharide products were then purified using a DEAE column. This process was repeated twice to ensure the completion of epimerization/2-*O*-sulfonation affording ^{13}C,^{15}N-labeled undersulfated heparin (-IdoA2S(1,4)GlcNS-). For 6-OST modification, ^{13}C,^{15}N-labeled undersulfated heparin (3 mg) was incubated with 6-OST-1 (26 mg, 80 units/μg) and 6-OST-3 (33 mg, 80 units/μg) in a total volume of 40 ml in the presence of components for PAPS regeneration system to afford ^{13}C,^{15}N-labeled heparin (-IdoA2S(1,4)GlcNS6S-). The extent of 6-*O*-sulfonation was also monitored by the disaccharide analysis. For 3-OST-1-modification step, the procedures were essentially same except for replacing 6-OST-1 and -3 with 3-OST-1 enzyme. The extent of 3-*O*-sulfonation was monitored by comparing the susceptibility of the 3-OST-1 modified *vs.* unmodified polysaccharide to additional 3-OST-1 modification using [^{35}S] PAPS.[2]

NMR. NMR samples were typically dissolved in 0.5 ml D_2O (99.996%, Sigma) and freeze-dried repeatedly to remove the exchangeable protons. The samples were re-dissolved in 0.3 ml of a D_2O based NMR buffer containing 10 mM sodium phosphate, and 20 mM NaCl. Spectra were recorded at 300K on Bruker Avance II 600 and 800 MHz spectrometers equipped with cryogenically cooled HCN-probes with z-axis gradients. In cases where water suppression was required, either selective irradiation of the water resonance during the relaxation delay or excitation sculpting was applied.[3] NOE intensities were normalized with respect to the diagonal peak at 0 mixing time. From the initial slopes, inter-proton distances were obtained by employing the isolated spin pair approximation, using the theoretical H1-H2 (for α-oriented $^4C_1$ chairs), H1-H3 (for α- or β- oriented $^4C_1$ chairs), H2-H4 (for α- or β- oriented $^4C_1$ chairs), and H1-H5 (for α- or β- oriented $^4C_1$ chairs) distances for the GlcNAc and/or GlcA moieties, where available or free of overlapping. In addition, a full matrix relaxation approach, using in-house software, was used to get the best match between the estimated and observed relative nOe intensities. For these calculations, the different basic conformers around the glycosidic linkages and for the IdoA ring derived from the MD or tar-MD simulations were employed as input geometries. All spectra were processed and analyzed using the programs TOPSPIN2.0 and Sparky (3.114), respectively.[4]

Disaccharide composition analysis of anticoagulant heparin. LC MS analyses were performed on Agilent 1100 LC/MSD instrument (Agilent Technologies, Inc. Wilmington, DE, U.S.A.) equipped with an ion trap, binary pump and a UV detector. The column was a 5 μm Zorbax SB-C18 (0.5 × 250 mm) from Agilent. Eluent A was water/acetonitrile (85:15), v/v and eluent B was water/acetonitrile (35:65) v/v. Both eluents contained 12 mM TBA and 38 mM NH_4OAc and their pH was adjusted to 6.5 with HOAc. The products of the heparin and anti-coagulant heparin were dissolved in 10 μl water and 1 μl of the resulting analyte was injected by auto-sampler. A gradient of 0% B for 15 min, and

following 0-50% B over 30 min. was used at a flow rate of 10 μl/min. Mass spectra were obtained using an Agilent 1100 series Classic G2445D LC/MSD trap. The electrospray interface was set in negative ionization mode with the skimmer potential -40.0 V, capillary exit -40.0 V and a source temperature of 325 °C to obtain maximum abundance of the ions in a full scan spectra (150–1500 Da, 10 full scans/s). Nitrogen was used as a drying (5 liters/min) and nebulizing gas (20 p.s.i.). Auto MS/MS was turned on in these experiments using an estimated cycle time of 0.07 min. Total ion chromatograms (TIC) and mass spectra were processed using Data Analysis 2.0 (Bruker Daltonics Inc., Billerica, MA).

APPT activity and ATIII-binding. $^{13}C,^{15}N$-labeled heparin and anticoagulant heparin (100 to 1500 ng) subjected to APTT assay and anticoagulant activity was calculated from a standard curve prepared using same concentrations of pharmaceutical heparin.[5] Binding of ^{35}S labeled anticoagulant heparin to ATIII-Sepharose was determined by scintillation counting. In ATIII-binding heparin, approximately 1×10^5 cpm of 3-*O*-[^{35}S]-labeled polysaccharide was incubated with 0.1 mg/ml human AT (Cutter Biological) in a buffer containing 10 mM Tris-HCl, pH 7.5, 150 mM NaCl, 1 mM Mn^{2+}, 1 mM Mg^{2+}, 1 mM Ca^{2+}, 10 μM dextran sulfate, 0.0004% Triton X-100, and 0.02% sodium azide for 30 min at room temperature. Concanavalin A (ConA)-Sepharose (Sigma, 50 μl of 1:1 slurry) was then added and the reaction was shaken at room temperature for 1 h. The beads were then washed by 3 × 1 ml binding buffer, and the bound polysaccharide was eluted with 1 M NaCl and counted.

MD-tar simulations in explicit water. NOE-derived distances were included as time-averaged distance constraints, using a $\langle r^{-6} \rangle^{-1/6}$ average. Final trajectories were run using an exponential decay constant of 400 ps and a simulation length of 4 ns for the MD-tar simulations. The use of explicit water molecules was absolutely required to get realistic conformers (see below for the protocol). Indeed, the use of a bulk dielectric constant (either fixed or distance-dependent), generated unrealistic heparin-like conformers with inter-strand contacts between different sugar rings. For undersulfated heparin and heparin, different simulations were submitted starting from the ^2S_O or $^1C_4$ conformer for the IdoA residue.

MD-tar simulations in explicit water. MD-tar simulations were performed with AMBER[6,7] 6.0 (parm94),[8] implemented with GLYCAM 06 parameters[9] and with parameters computed for the sulfo and sulfamo groups,[10] to accurately simulate the conformational behavior of the sugar moiety and the sulfo and sulfamo groups, respectively. NOE-derived distances were included as time-averaged distance constraints, using a $\langle r^{-6} \rangle^{-1/6}$ average. Final trajectories were run using an exponential decay constant of 400 ps and a simulation length of 4 ns for the MD-tar simulations. The use of explicit water molecules was absolutely required to get realistic conformers (see below for the protocol). Indeed, the use of a bulk dielectric constant (either fixed or distance-dependent), generated unrealistic heparin-like conformers with inter-strand contacts

between different sugar rings. For undersulfated heparin and heparin, different simulations were submitted starting from the $^{2}S_{O}$ or $^{1}C_{4}$ conformer for the IdoA residue.

Molecular modeling without restraints in explicit water. Equilibration of the system was carried out as follows; as a first step, a short minimization with positional restraints on solute by a harmonic potential with a force constant of 500 kcal·mol^{-1}·Å^{-2} was done. A 12.5 ps molecular dynamics calculation at 300 K maintaining positional restraints on the solute was then run to equilibrate the water box. For these two steps, a 9Å cut-off was used for the treatment of the electrostatic interactions. The system was equilibrated during an additional 12.5 ps period, but now using the mesh Ewald method, as water properties are slightly different with this treatment. The system was then subjected to several minimization cycles during which the force constant for positional restraints on the solute were gradually reduced from 500 to 0 kcal·mol^{-1}·Å^{-2}. Unrestrained MD trajectories at constant pressure (1 atm) and temperature (300 K) were collected and analyzed using the CARNAL module of AMBER. The simulation length was 7−9 ns. For undersulfated heparin and heparin, different simulations were submitted starting from the skew boat or chair conformers for the IdoA ring. The analysis of the trajectories, overlays, and RMDS calculations were performed using the free MOLMOL[58] and PyMOL program (DeLano Scientific LLC).

References

1. Vann, W.F., Schmidt, M.A., Jann, B., Jann, K. *Eur. J. Biochem*. **1981**, *116*, 359-364.
2. Chen, J., Avci, F.Y., Munoz, E.M., McDowell, L.M., Chen, M., Pedersen, L.C., Zhang, L., Linhardt, R.J., Liu, J. *J. Biol. Chem.* **2005**, *280*, 42817-42825.
3. Hwang, T.-L., Shaka, A.J., *J. Magn. Reson.* Series A **1995**, *112*, 275-279.
4. Zhang, L., Yang, D. *Bioinformatics* **2006**, *15*, 22, 2833-2834.
5. Murugesan, S., Park, T.J., Yang, H., Mousa, S., Linhardt, R.J. *Langmuir* **2006**, *22*, 3461-3463.
6. Pearlman, D.A., Case, D.A., Caldwell, J.W., Ross, W.R., Cheatham III, T.E., DeBolt, S., Ferguson, D., Seibel, G., Kollman, P. *Comp. Phys. Commun.* **1995**, *91*, 1-41.
7. Kollman, P.A. **1999**, University of California, San Francisco.
8. Cornell, W.D., Cieplak, P., Bayly, C.I., Gould, I.R., Merz, K.M., Ferguson, D.M., Spellmeyer, D.C., Fox, T., Caldwell, J.W., Kollman, P.A. *J. Am. Chem. Soc.* **1995**, *117*, 5179–5197.
9. Woods, R.J., Dwek, R.A., Edge, C.J., Fraser-Reid, B. *J. Phys. Chem. B*. **1995**, *99*, 3832–3846.
10. Lan, J., **2007**, Ph.D. Thesis, University of Edinburgh.
11. Koradi, R., Billeter, M., Wüthrich, K. *J. Mol. Graphics*, **1996**, *14*, 51-55.

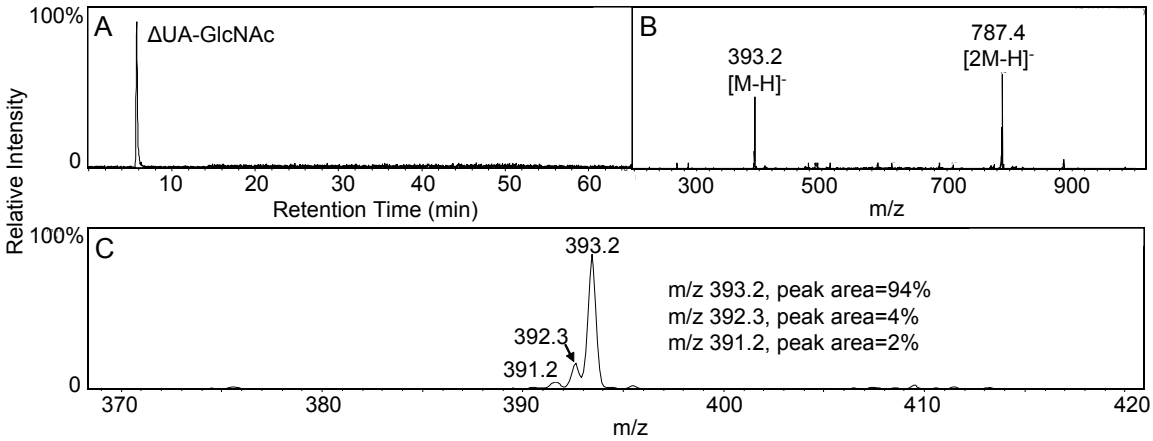

Figure S1. HPLC-ESI-MS disaccharide analysis of *N*-acetylheparosan. A, Total ion chromatography (TIC) of *N*-acetylheparosan; B, ESI-MS of *N*-acetylheparosan in negative mode; C: Magnified ESI-MS of *N*-acetylheparosan, fully enriched $^{13}C_{15}{}^{14}N_1{}^{16}O_{11}{}^{1}H_{21}$=94%.

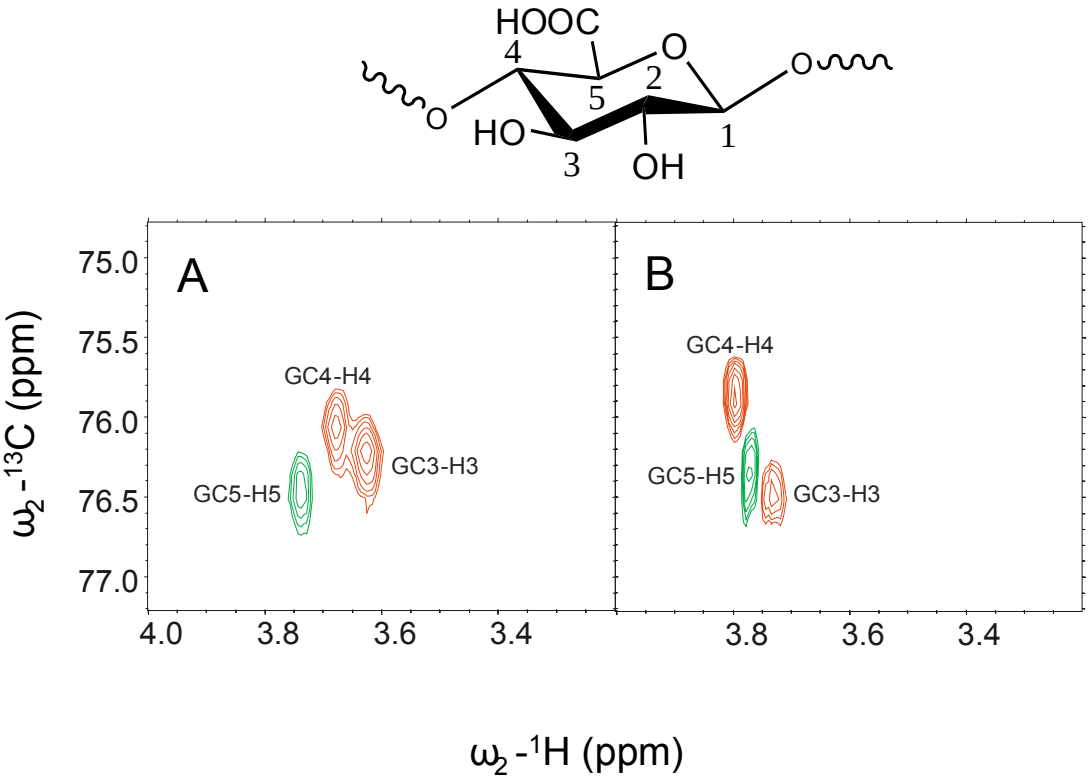

Figure S2 Constant-time HSQC of *N*-acetyl and *N*-sulfoheparosan. A, *N*-acetylheparosan; B: *N*-sulfoheparosan.

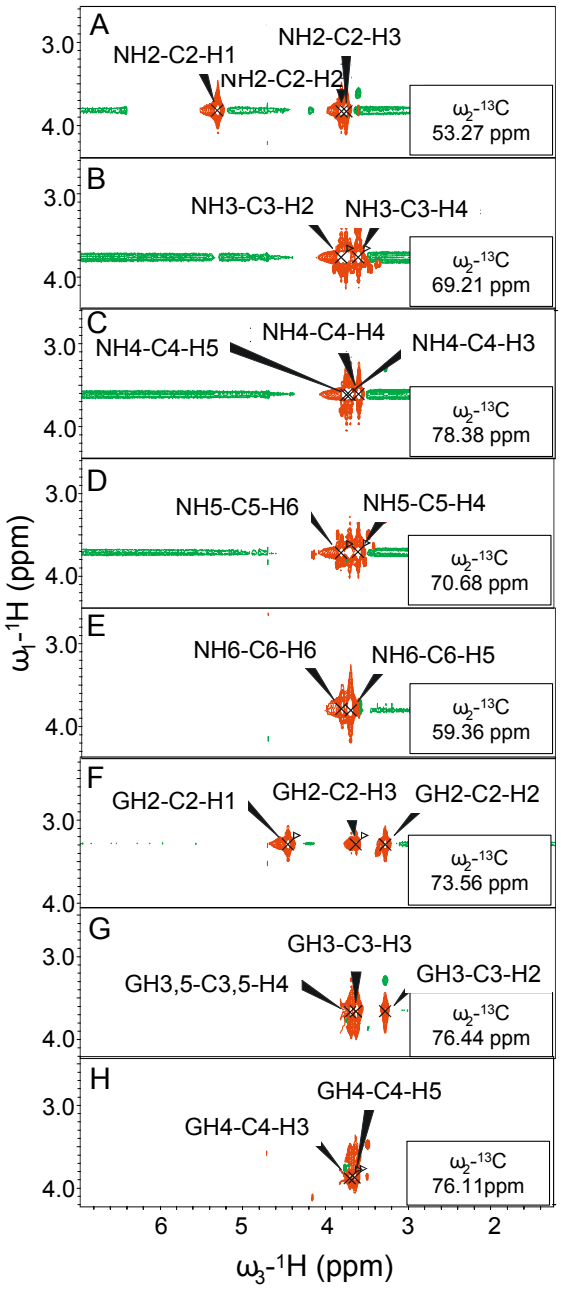

Figure S3. Strip plots from the 3D-HCCH-COSY spectrum of ^{13}C, ^{15}N-labeled *N*-acetylheparosan. Panels **A** through **E** illustrate a sequential walk from C2 of GlcN to C6 of GlcN; Panels **F** through **H** under C2 of GlcA to C5 of GlcA.

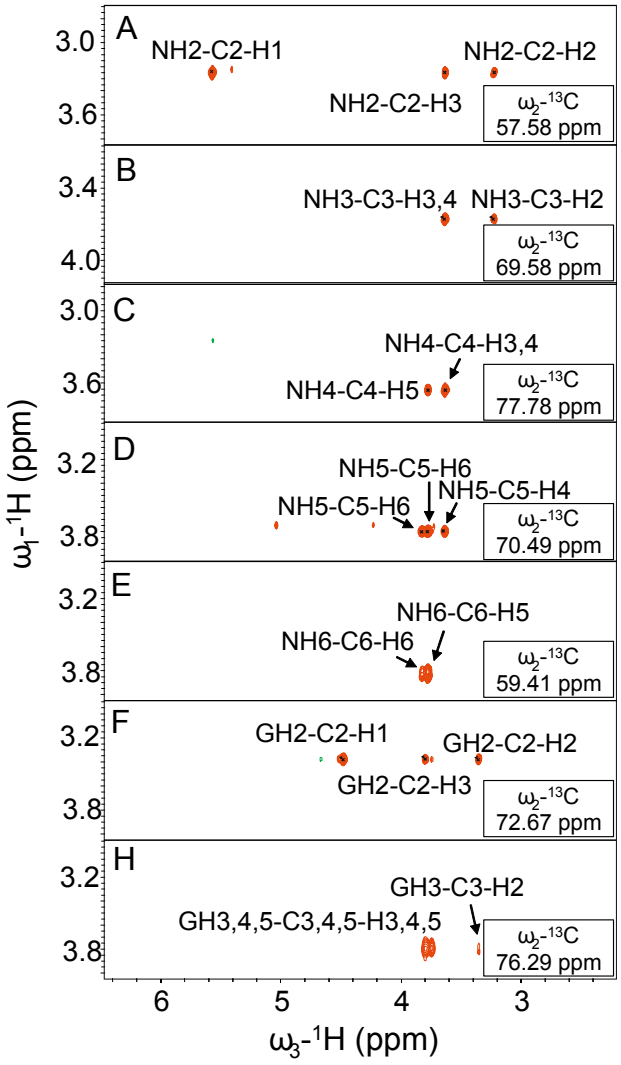

Figure S4. Strip plots from the 3D-HCCH-COSY spectrum of ^{13}C, ^{15}N-labeled *N*-sulfoheparosan. Panels **A** through **E** illustrate a sequential walk from C2 of GlcN to C6 of GlcN; Panels **F** and **H** under C2 of GlcA to C5 of GlcA.

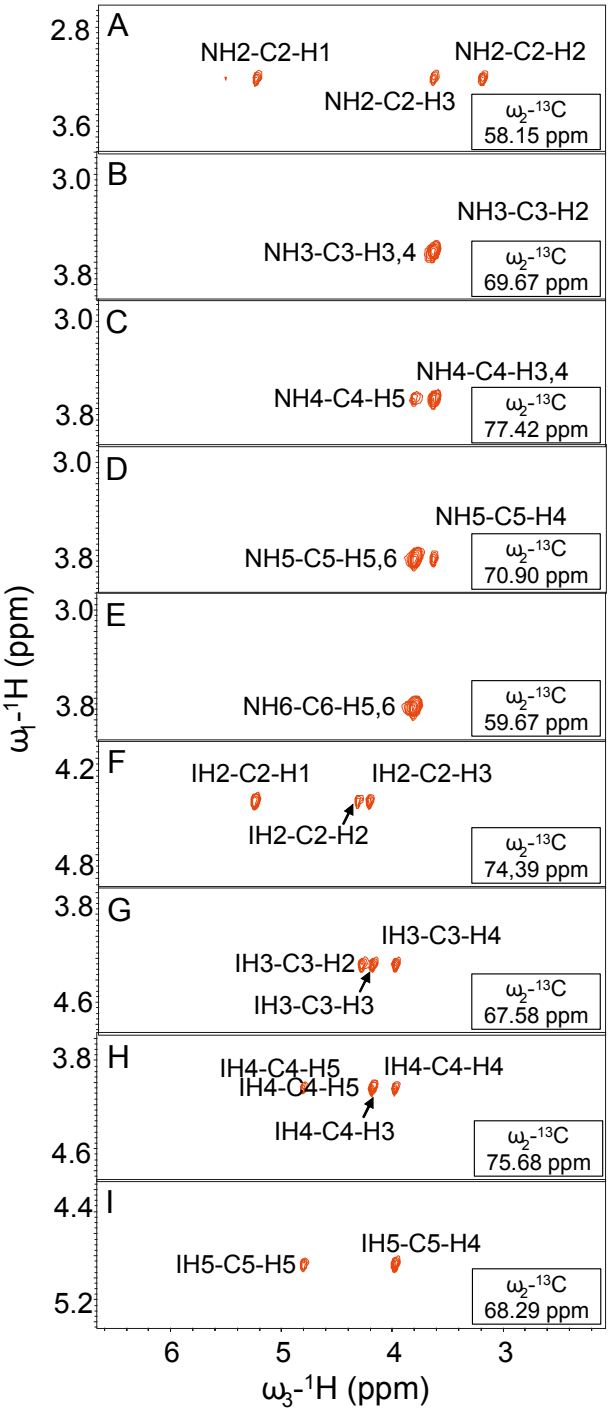

Figure S5. Strip plots from the 3D-HCCH-COSY spectrum of ^{13}C, ^{15}N-labeled undersulfated heparin. Panels **A** through **E** illustrate a sequential walk from C2 of GlcN to C6 of GlcN; Panels **F** through **I** under C2 of IdoA to C5 of IdoA.

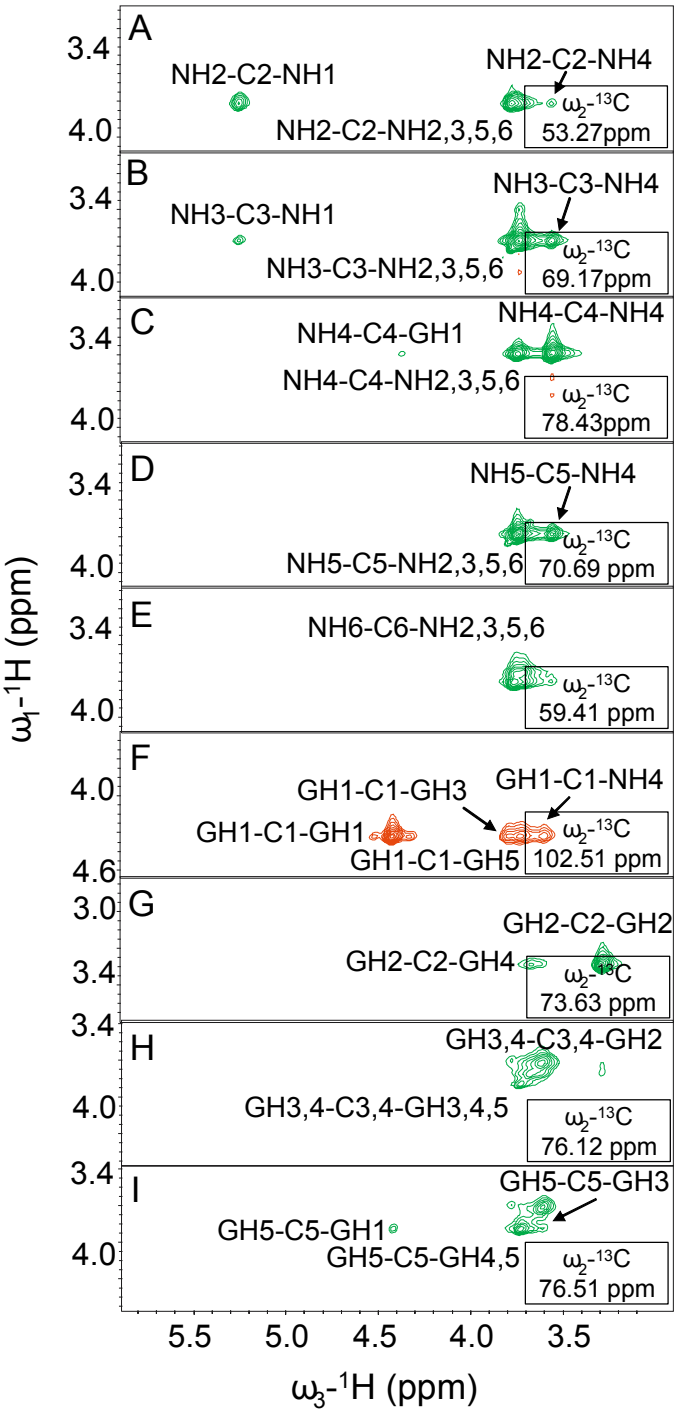

Figure S6. Strip plots from the 3D-HCCH-nOes spectrum of ^{13}C, ^{15}N-labeled *N*-acetylheparosan. Panels **A** through **E** illustrate a sequential walk from C2 of GlcN to C6 of GlcN; Panels **F** through **I** under C1,2,4,5 of GlcA.

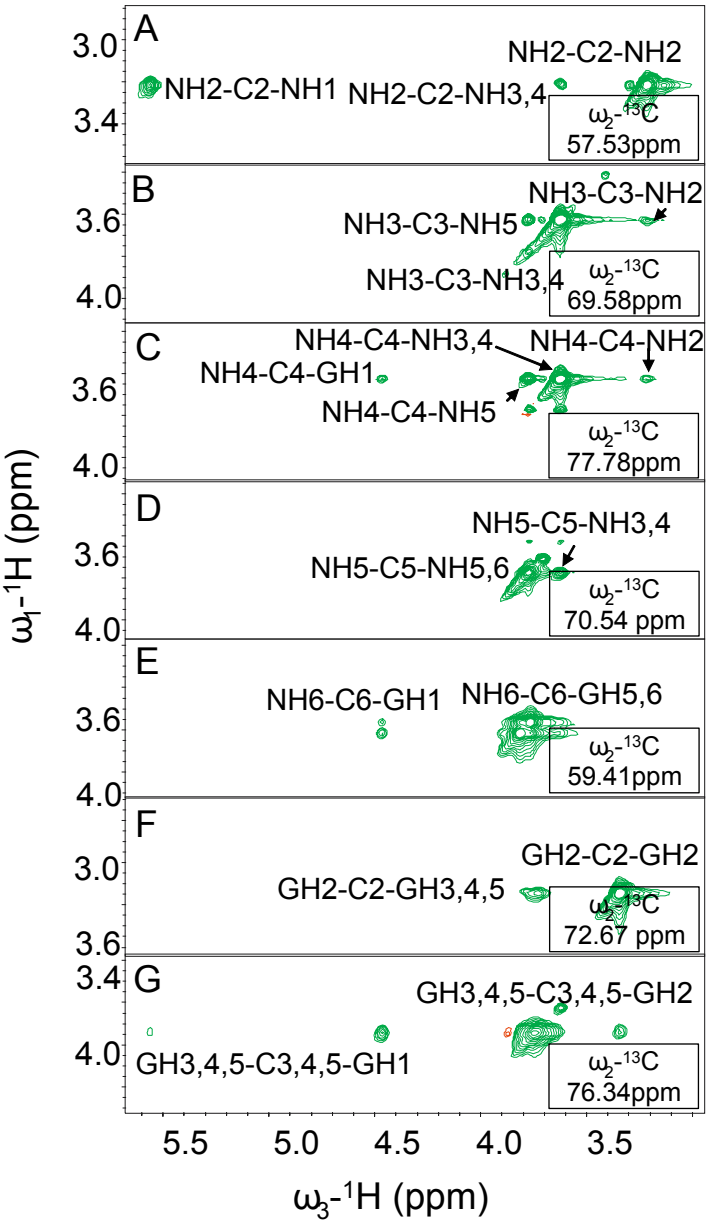

Figure S7. Strip plots from the 3D-HCCH-nOes spectrum of ^{13}C, ^{15}N-labeled *N*-sulfoheparosan. Panels **A** through **E** illustrate a sequential walk from C2 of GlcN to C6 of GlcN; Panels **F** and G under C2, 3, 4, 5 of GlcA.

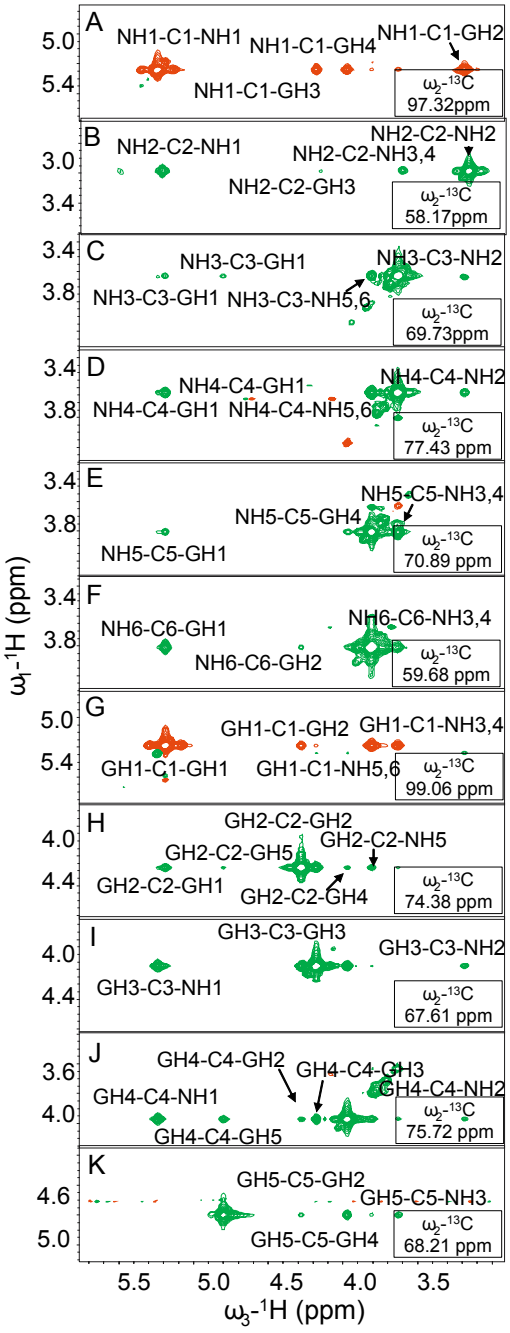

Figure S8. Strip plots from the 3D-HCCH-nOes spectrum of ^{13}C, ^{15}N-labeled undersulfated heparin. Panels **A** through **F** illustrate a sequential walk from C1 of GlcN to C6 of GlcN; Panels **G** and K under C1 to C5 of IdoA.

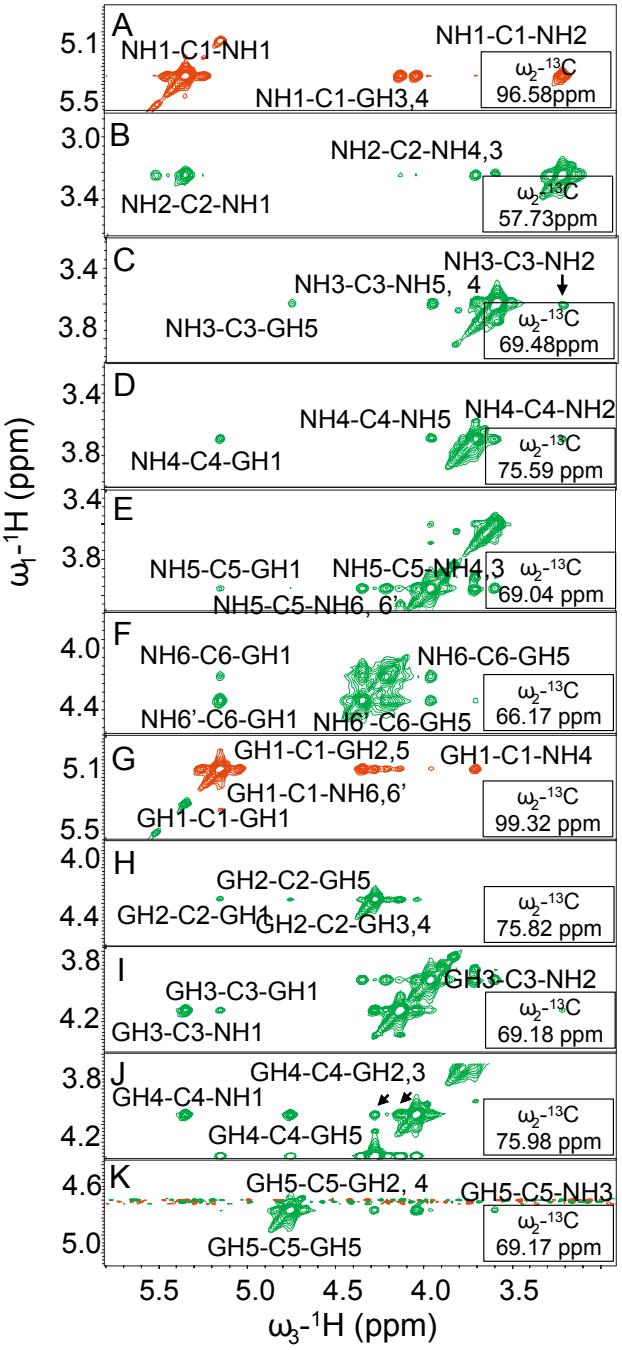

Figure S9. Strip plots from the 3D-HCCH-nOes spectrum of ^{13}C, ^{15}N-labeled heparin. Panels **A** through **F** illustrate a sequential walk from C1 of GlcN to C6 of GlcN; Panels **G** and K under C1 to C5 of IdoA.

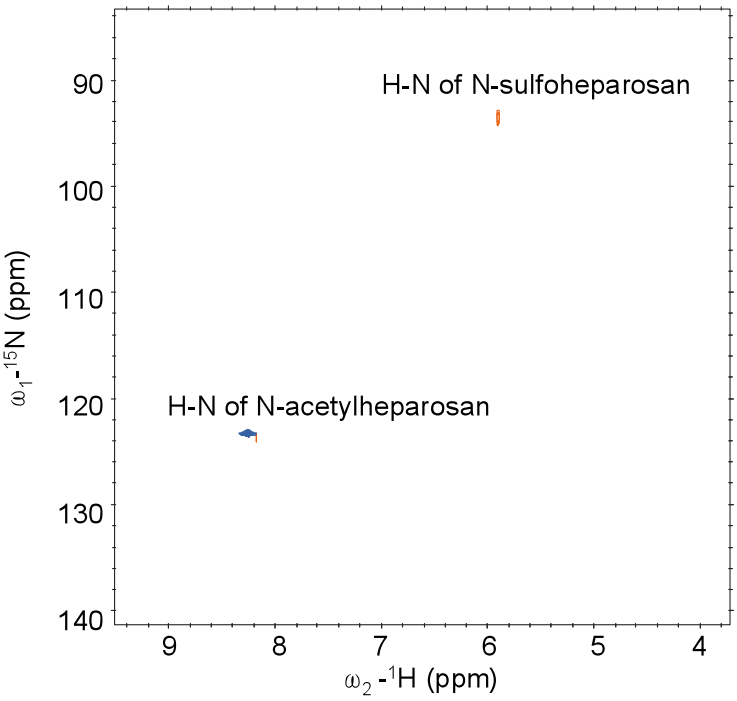

Figure S10. H-N HSQC of ^{13}C, ^{15}N-labeled *N*-acetyl and sulfated heparosan.

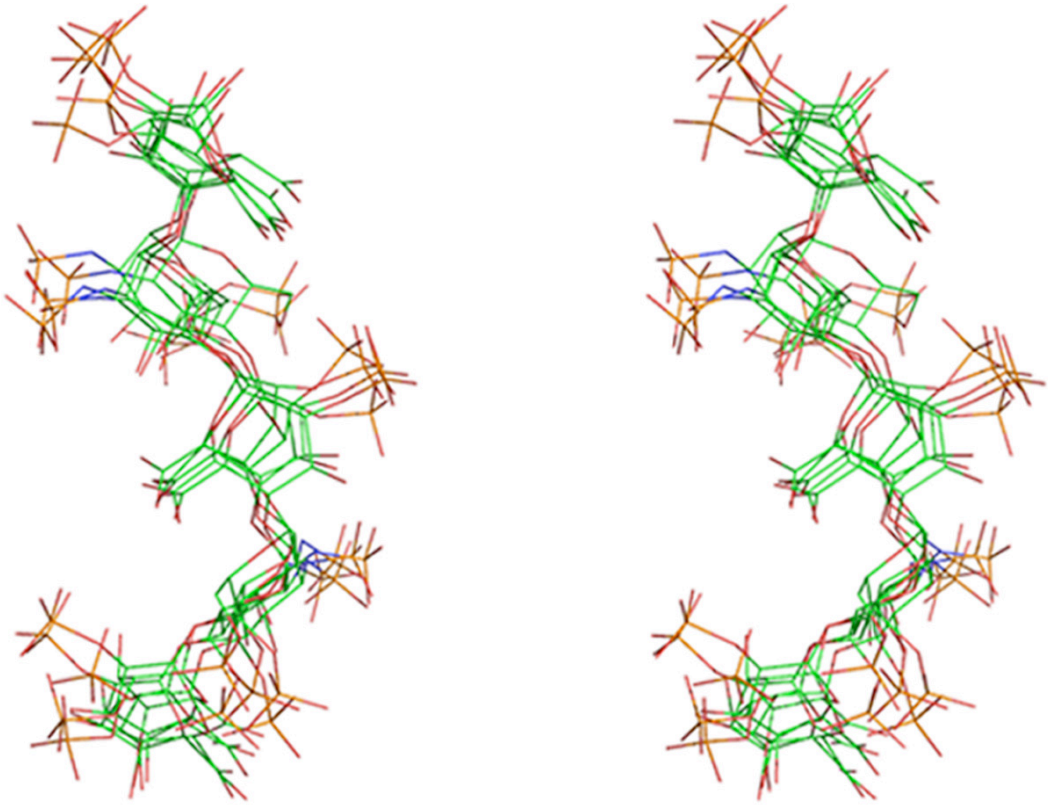

Figure S11. Stereoview of heparin helix. Five members from the ensemble used to make Fig. 4D were randomly selected and the terminal sugar at each end was removed. This is a 'wall-eyed' figure and requires stero glasses (crossing eyes inverts parts of the image and makes sites contorted).

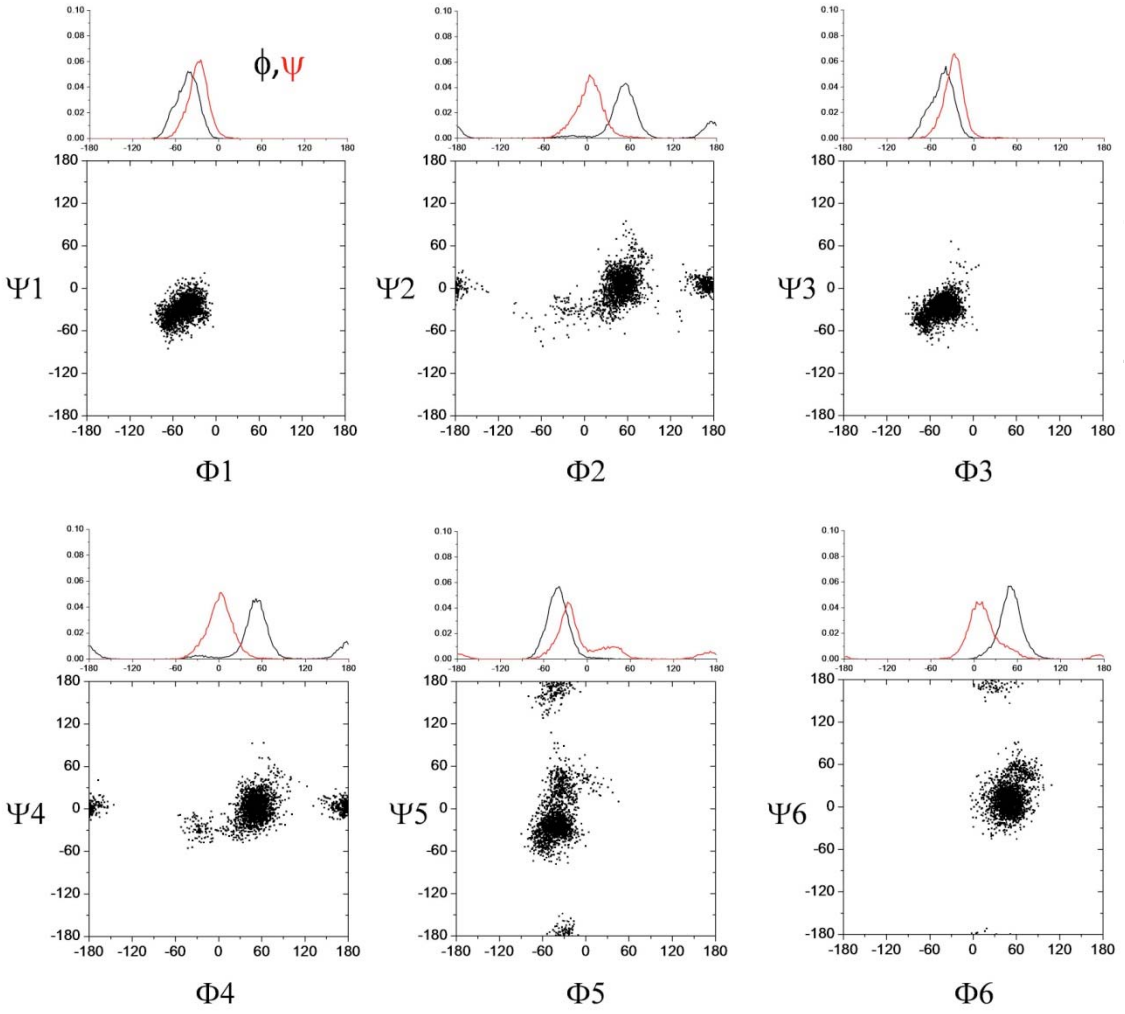

Figure S12. The F/Y distributions for the glycosidic torsions of *N*-acetyl heparosan, as estimated by tar-MD simulations (4 ns of simulation time) in explicit water, and employing the NOE-derived distances as experimental tar-restraints ($<r^{-3}>^{-1/3}$). The distributions for the two glycosidic angles are also given above the corresponding map. In general, the conformational space for each torsion is well defined, although a certain degree of flexibility is again evidenced.

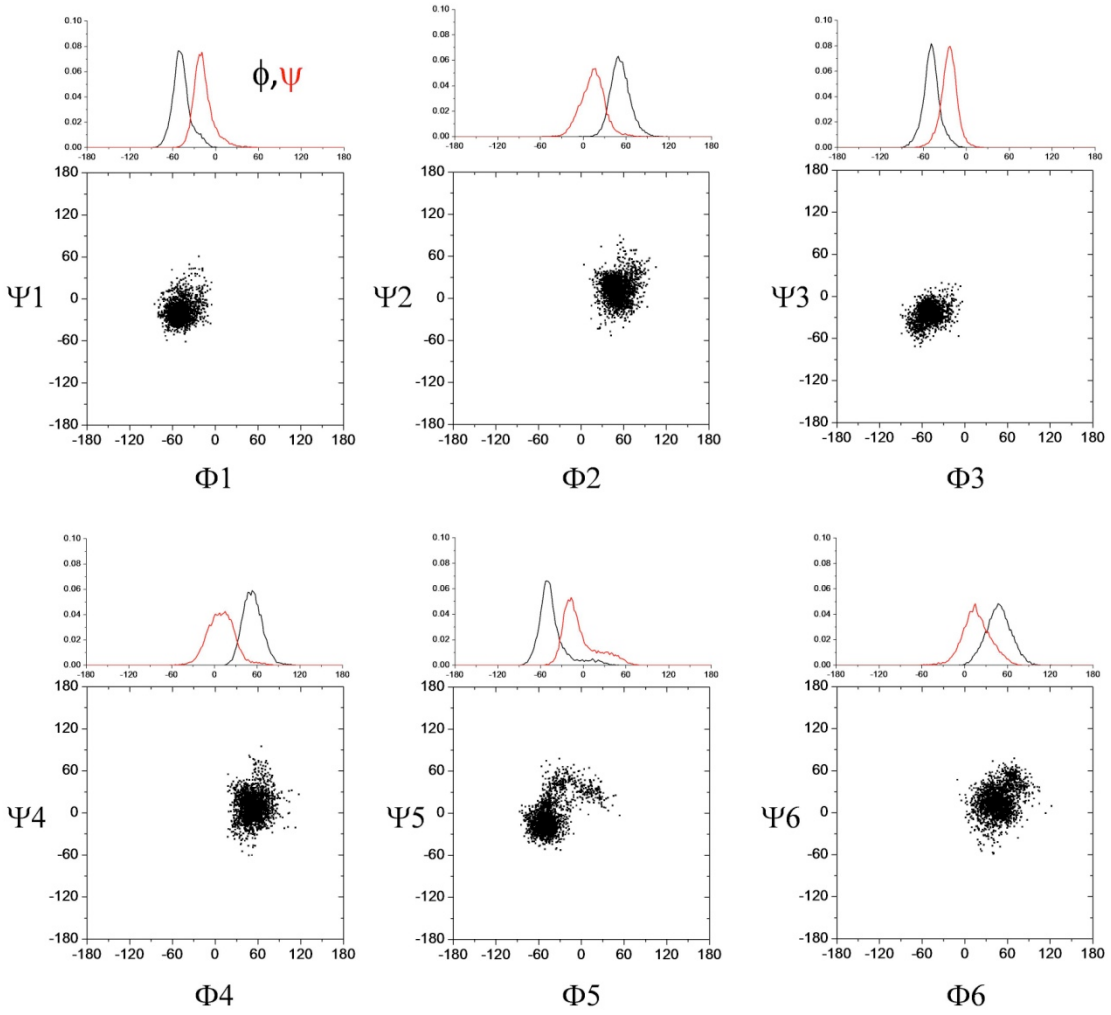

Figure S13. The Φ/Ψ distributions for the glycosidic torsions of *N*-sulfoheparosan, as estimated by tar-MD simulations (4 ns of simulation time) in explicit water, and employing the NOE-derived distances as experimental tar-restraints ($<r^{-3}>^{-1/3}$). The distributions for the two glycosidic angles are also given above the corresponding map. In general, the conformational space for each torsion is well defined, although a certain degree of flexibility is again evidenced.

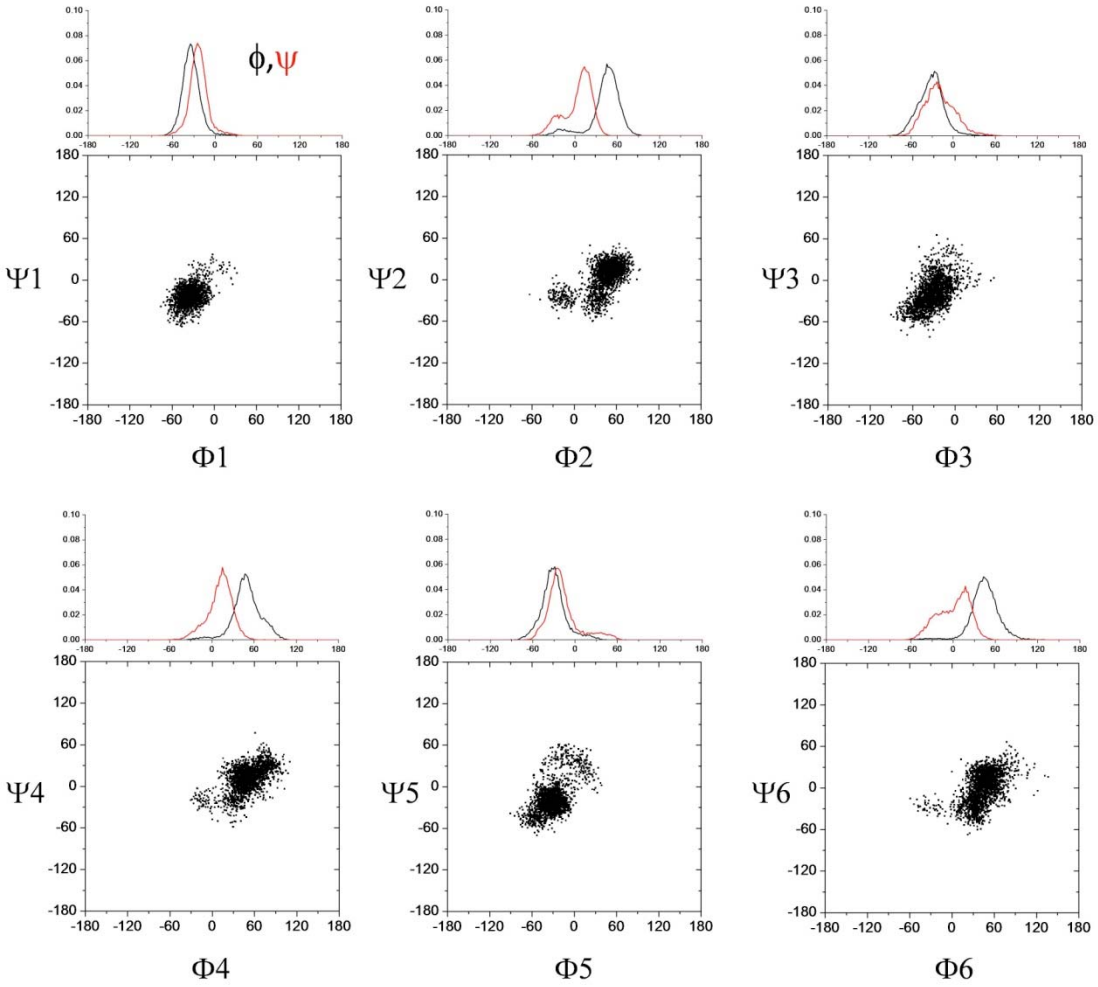

Figure S14. The Φ/Ψ distributions for the glycosidic torsions of undersulfated heparin, as estimated by MD simulations (4 ns of simulation time) in explicit water, and employing the NOE-derived distances as experimental tar-restraints ($<r^{-3}>^{-1/3}$). The starting conformation of the L-Ido rings was the $^{1}C_{4}$ chair conformer. The distributions for the two glycosidic angles are also given above the corresponding map. In general, the conformational space for each torsion is well defined, although a certain degree of flexibility is again evidenced.

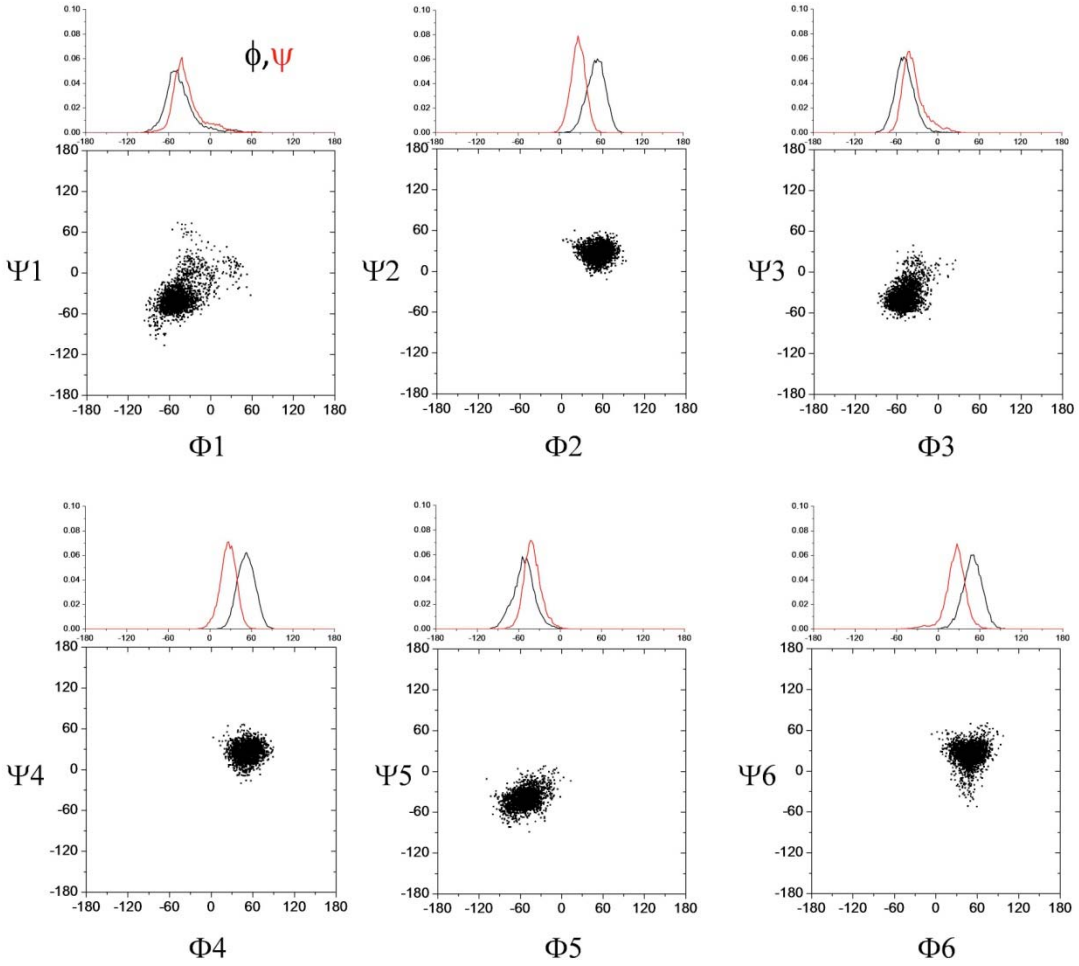

Figure S15. The Φ/Ψ distributions for the glycosidic torsions of heparin, as estimated by MD simulations (4 ns of simulation time) in explicit water, and employing the NOE-derived distances as experimental tar-restraints ($<r^{-3}>^{-1/3}$). The starting conformation of the L-Ido rings was the $^{1}C_{4}$ chair conformer.The distributions for the two glycosidic angles are also given above the corresponding map. In general, the conformational space for each torsion is well defined, although a certain degree of flexibility is again evidenced.

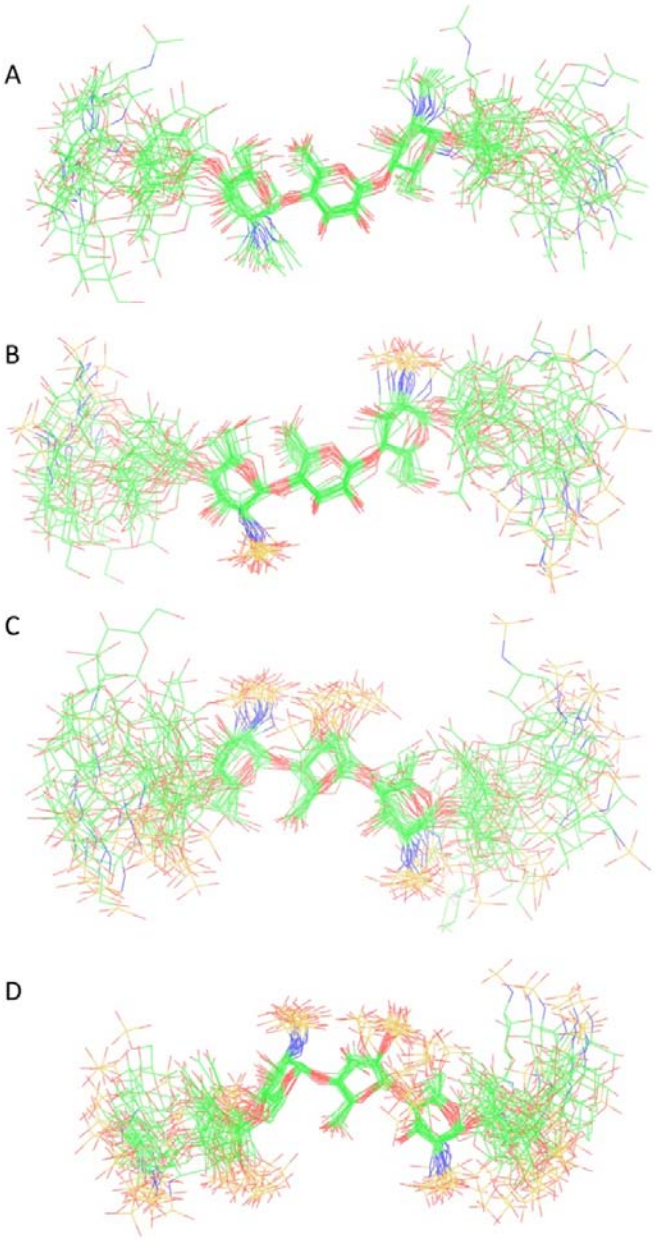

Figure S16. Superimposition of 20 conformers randomly taken from the tar-MD simulations, employing the NOE-derived distances as experimental tar-restraints ($<r^{-3}>^{-1/3}$), for each GAG. The central residues have been chosen for the superimposition to show the propagation of the flexibility around the GAG chain. **A**. *N*-acetylheparosan; **B**. *N*-sulfoheparosan; **C**. undersulfated heparin; and **D**. heparin. Carbon is shown in green, oxygen in red, nitrogen in blue and sulfur in yellow.

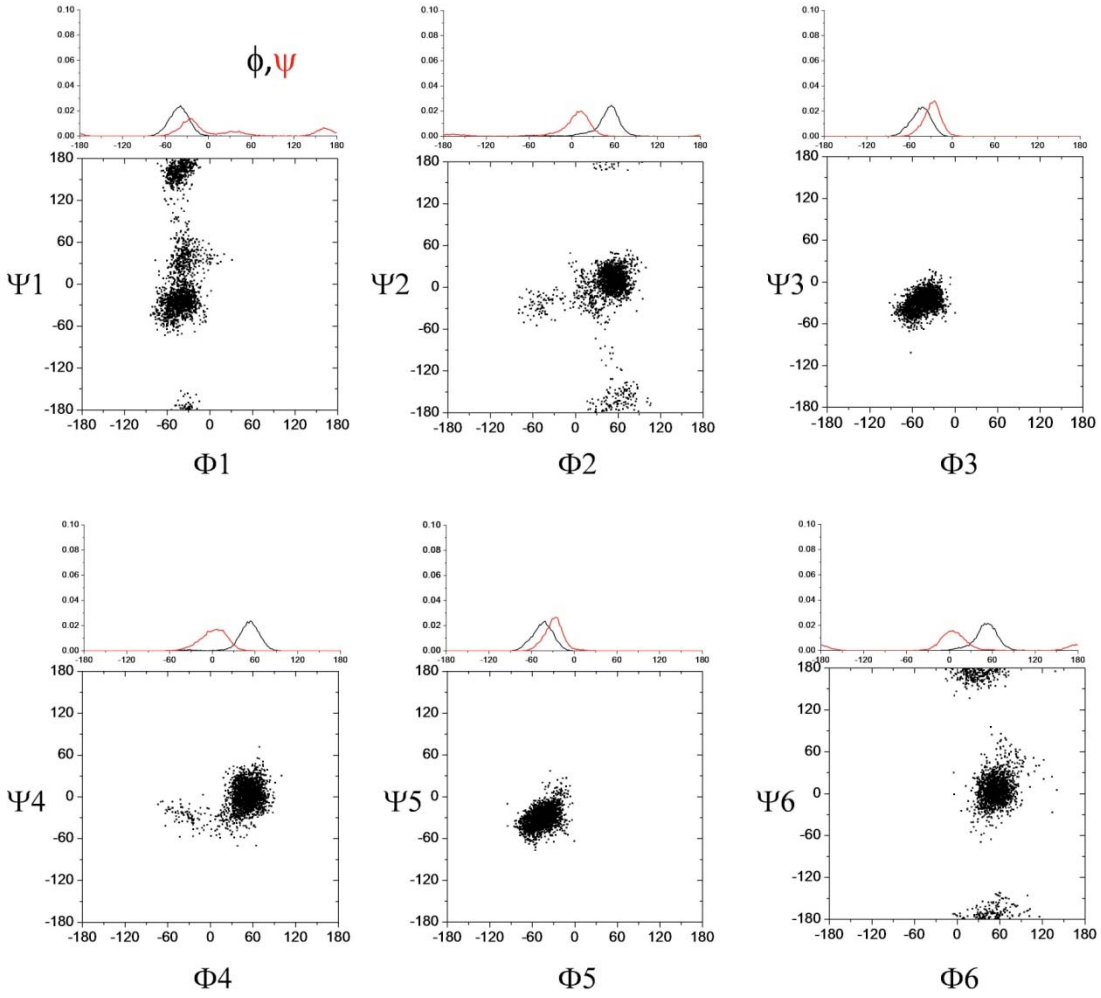

Figure S17. The Φ/Ψ distributions for the glycosidic torsions of *N*-acetylheparosan, as estimated by MD simulations (4 ns of simulation time) in explicit water, and employing the NOE-derived distances as experimental tar-restraints ($<r^{-6}>^{-1/6}$). The distributions for the two glycosidic angles are also given above the corresponding map. In general, the conformational space for each torsion is well defined, although a certain degree of flexibility is again evidenced.

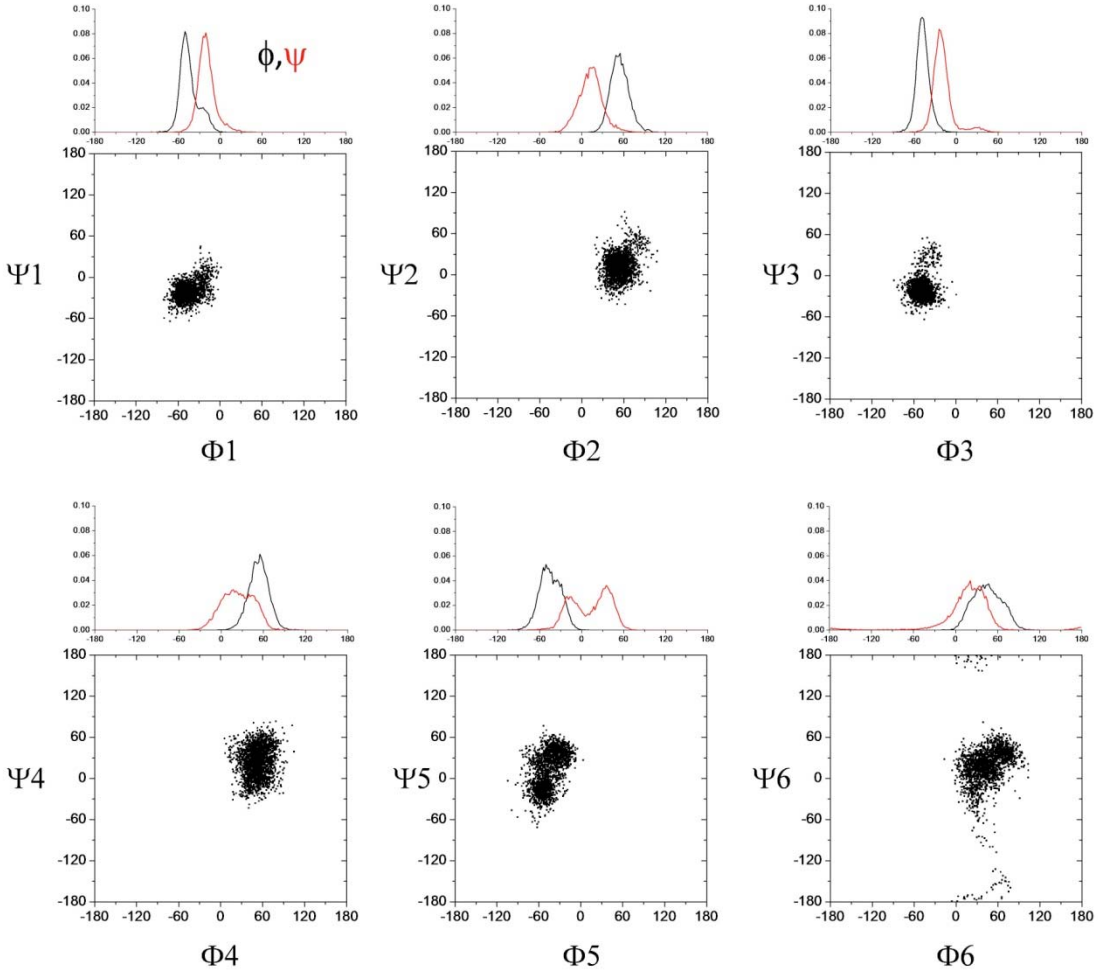

Figure S18. The Φ/Ψ distributions for the glycosidic torsions of *N*-sulfoheparosan, as estimated by tar-MD simulations (4 ns of simulation time) in explicit water, and employing the NOE-derived distances as experimental tar-restraints ($<r^{-6}>^{-1/6}$). The distributions for the two glycosidic angles are also given above the corresponding map. In general, the conformational space for each torsion is well defined, although a certain degree of flexibility is again evidenced.

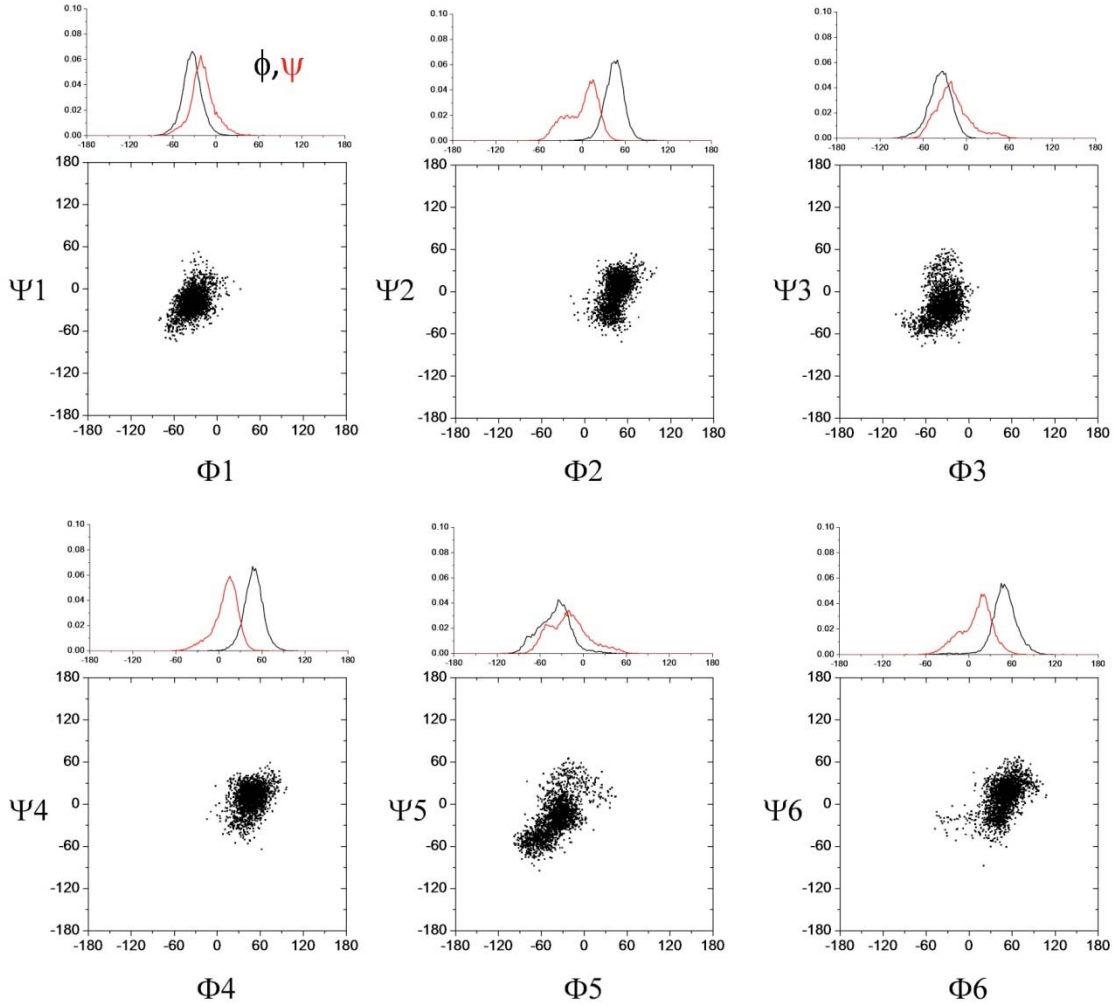

Figure S19. The Φ/Ψ distributions for the glycosidic torsions of undersulfated heparin, as estimated by MD simulations (4 ns of simulation time) in explicit water, and employing the NOE-derived distances as experimental tar-restraints ($<r^{-6}>^{-1/6}$). The starting conformation of the L-Ido rings was the $^{1}C_{4}$ chair conformer. The distributions for the two glycosidic angles are also given above the corresponding map. In general, the conformational space for each torsion is well defined, although a certain degree of flexibility is again evidenced.

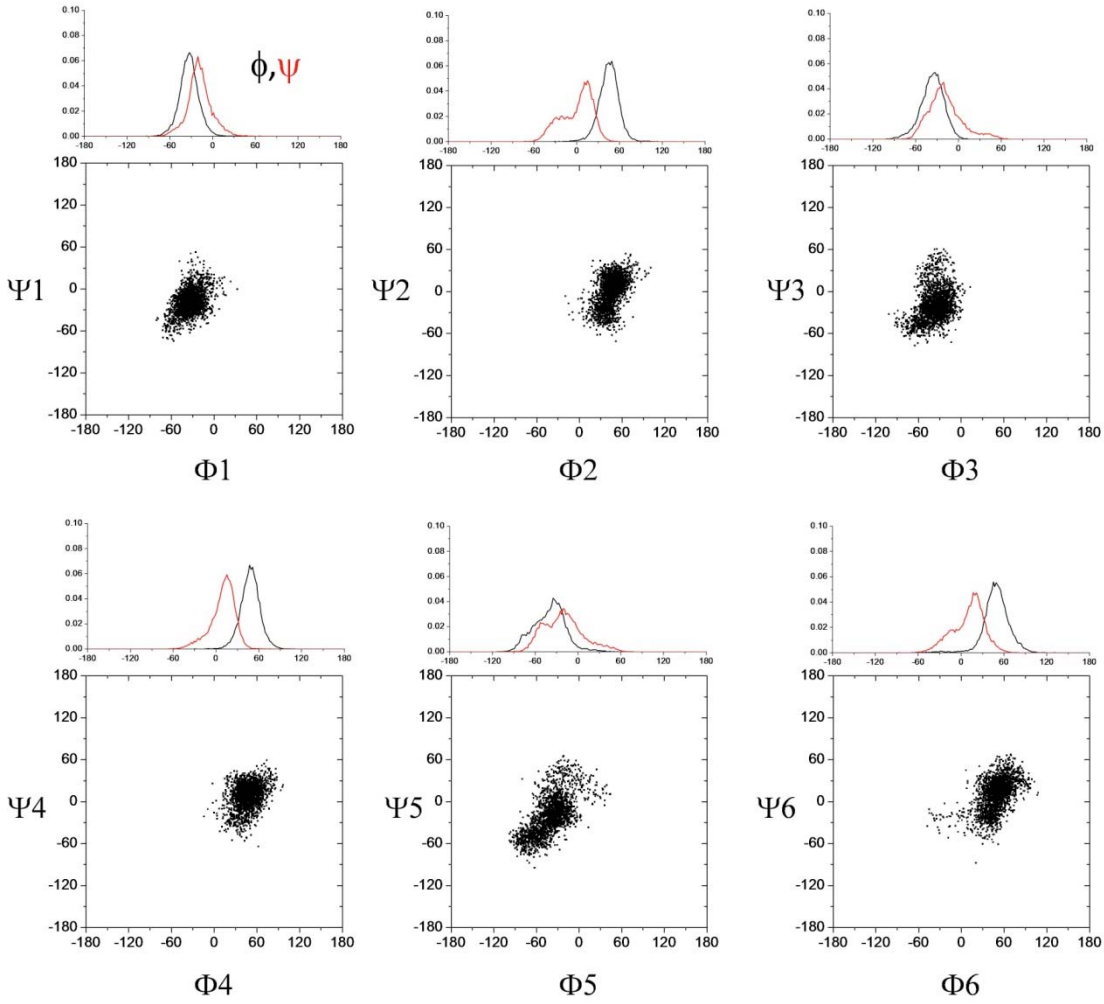

Figure S20. The Φ/Ψ distributions for the glycosidic torsions of heparin, as estimated by MD simulations (4 ns of simulation time) in explicit water, and employing the NOE-derived distances as experimental tar-restraints ($<r^{-6}>^{-1/6}$). The starting conformation of the L-Ido rings was the $^{1}C_{4}$ chair conformer.The distributions for the two glycosidic angles are also given above the corresponding map. In general, the conformational space for each torsion is well defined, although a certain degree of flexibility is again evidenced.

Table S1. Disaccharide composition analysis of $^{13}C,^{15}N$ heparin and anticoagulant heparin determined using HPLC-ESI-MS.

Structure	Retention time (min)	Ratio	
		Heparin	Anticoagulant heparin
ΔUA-GlcNS	8.0	1.6%	2.3%
ΔUA-GlcNS6S	20.0	4.9%	2.5%
ΔUA2S-GlcNS	26.0	4.5%	2.3%
ΔUA2S-GlcNS6S	42.5	89%	86.1%
Total peak area		100%	93.2%

Table S2. The results of the tar-MD simulations ($<r^{-3}>^{-1/3}$ averaging) for the different glycosidic linkages of *N*-acetylheparosan. The experimental key proton-pair distances (Å) as deduced from the NOE-based 3D NOESY-HSQC experiments were implemented as tar-contraints with a 10% margin. No stereospecific assignment was performed and the restraint was set to the corresponding C-6 carbon atom (adding 0.8 Å).

	H1 GlcA- H4 GlcNAc	**H1 GlcA- H3 GlcNAc**	**H1 GlcA- H6[a] GlcNAc**	**H1 GlcA- H6[b] GlcNAc**	**H1 GlcNAc- H4 GlcA**	**H1 GlcNAc- H3 GlcA**
1→2	--	--	--	--	2.5	3.4
2→3	2.6	4.4	2.9	2.9	--	--
3→4	--	--	--	--	2.5	3.4
4→5	2.6	4.4	3.0	2.9	--	--
5→6	--	--	--	--	2.5	3.3
6→7	2.5	4.2	2.7	2.6	--	--
MD-average	2.6	4.3	2.9	2.8	2.5	3.4
experimental	*2.5*	*4.5*	*2.7**	*2.7**	*2.5*	*2.6*

Table S3. The results of the tar-MD simulations ($<r^{-3}>^{-1/3}$ averaging) for the different glycosidic linkages of *N*-sulfoheparosan. The experimental key proton-pair distances (Å) as deduced from the NOE-based 3D NOESY-HSQC experiments were implemented as tar-contraints with a 10% margin. No stereospecific assignment was performed and the restraint was set to the corresponding C-6 carbon atom (adding 0.8 Å).

	H1 GlcA- H4 GlcNS	**H1 GlcA- H3 GlcNS**	**H1 GlcA- H6[a] GlcNS**	**H1 GlcA- H6[b] GlcNS**	**H1 GlcNS- H4 GlcA**	**H1 GlcNS- H3 GlcA**
1→2	--	--	--	--	2.5	3.6
2→3	2.5	4.5	2.7	2.5	--	--
3→4	--	--	--	--	2.6	3.5
4→5	2.5	4.5	2.5	2.7	--	--
5→6	--	--	--	--	2.4	3.7
6→7	2.5	4.5	2.9	2.5	--	--
MD-average	2.5	4.5	2.7	2.6	2.5	3.6
experimental	*2.7*	*4.5*	*2.5**	*2.5**	*2.7*	*3.8*

Table S4. The results of the tar-MD simulations ($<r^{-3}>^{-1/3}$ averaging) for the different glycosidic linkages of undersulfated heparin. The experimental key proton-pair distances (Å) as deduced from the NOE-based 3D NOESY-HSQC experiments were implemented as tar-contraints with a 10% margin. No stereospecific assignment was performed and the restraint was set to the corresponding C-6 carbon atom (adding 0.8 Å).

	H1 IdoA- H4 GlcNS	**H1 IdoA- H3 GlcNS**	**H1 IdoA- H6[a] GlcNS**	**H1 IdoA- H6[b] GlcNS**	**H1 GlcNS- H4 IdoA**	**H1 GlcNS- H3 IdoA**
1→2	--	--	--	--	2.3	2.6
2→3	2.3	4.3	2.6	2.8	--	--
3→4	--	--	--	--	2.2	2.7
4→5	2.4	4.4	2.6	2.6	--	--
5→6	--	--	--	--	2.2	2.6
6→7	2.3	4.3	2.6	3.2	--	--
MD-average	2.3	4.3	2.6	2.9	2.2	2.6
experimental	*2.5*	*4.5*	*2.7**	*2.7**	*2.5*	*2.7*

Table S5. The results of the tar-MD simulations ($<r^{-3}>^{-1/3}$ averaging) for the different glycosidic linkages of heparin. The experimental key proton-pair distances (Å) as deduced from the NOE-based 3D NOESY-HSQC experiments were implemented as tar-contraints with a 10% margin. No stereospecific assignment was performed and the restraint was set to the corresponding C-6 carbon atom (adding 0.8 Å).

	H1 IdoA- H4 GlcNS	**H1 IdoA- H3 GlcNS**	**H1 IdoA- H6[a] GlcNS**	**H1 IdoA- H6[b] GlcNS**	**H1 GlcNS- H4 IdoA**	**H1 GlcNS- H3 IdoA**
1→2	--	--	--	--	2.6	2.6
2→3	2.6	4.5	2.2	3.7	--	--
3→4	--	--	--	--	2.6	2.6
4→5	2.6	4.5	2.2	3.7	--	--
5→6	--	--	--	--	2.7	2.5
6→7	2.6	4.4	2.3	3.8	--	--
MD-average	2.6	4.5	2.2	3.7	2.6	2.6
experimental	*2.4*	*4.5*	*2.6**	*3.1**	*2.8*	*2.8*

Table S6. Comparison of experimental and calculated nOes for the different polysaccharides, as deduced from the 3D NOESY-HSQC experiments at 20, 40 and 100 ms mixing times. The data shown in the table correspond to the experiment with 40 ms mixing time. The integrals estimated for the other experiments followed the same trend. The experimental data were estimated from the integrals of the cross peaks to the integral of the corresponding diagonal peak (the HSQC-based cross peak for the plane under study). For any given proton pair, there are two planes for which the intensities can be measured. The given values are averaged for both planes when no overlapping was present. In the case of overlapping peaks, the data correspond to those estimated from the alternative plane. The estimated experimental error is ± 20%. For the calculated nOes, a symmetric top model was considered with correlation time values of $t_{\perp}$ of 8 ns and $t_{\parallel}$ of 0.16 ns was employed, as described in reference 12. It was impossible to simultaneously fit all data using isotropic motional model (see details in Table for heparin), especially those for the H1 IdoA- H2 IdoA and H1 IdoA- H4 GlcNS linkages, whose corresponding vectors lie perpendicular to the main axis. Analogous observations take place for the other three polysaccharides, with the H1 GlcA- H2 GlcA and H1 GlcA- H4 GlcNS linkages in the heparosan.

	H1 GlcA-H4 GlcNAc	**H1 GlcA – H6 GlcNAc***	**H1 GlcNAc-H3 GlcA**	**H1 GlcNAc-H4 GlcA**	**H1 GlcNAc -H2 GlcNAc**	**H1 GlcA -H2 GlcA**
***N*-acetylheparosan**						
EXPERIMENTAL	-6%	-10%	-12%	-2%	-20%	-5%
CALCULATED‡	-5%	-11%	-13%	-3%	-22%	-5%
***N*-sulfoheparosan**						
EXPERIMENTAL	-5%	-15%	-14%	-2%	-31%	-8%
CALCULATED‡	-3%	-15%	-17%	-2%	-28%	-8%
	H1 IdoA-H4 GlcNS	**H1 IdoA-H6 GlcNS***	**H1 GlcNS-H3 IdoA**	**H1 GlcNS-H4 IdoA**	**H1 GlcNS-H2 GlcNS-**	**H1 IdoA-H2 IdoA**
Undersulfated Heparin						
EXPERIMENTAL	-8%	-10%	-30%	-5%	-26%	-6%
CALCULATED‡	-6%	-15%	-34%	-5%	-21%	-6%
Heparin						
EXPERIMENTAL	-7%	-14%	-14%	-18%	-36%	-6%
CALCULATED (ensemble average) (symmetric top)	-6%	-12%	-12%	-22%	-28%	-5%
CALCULATED (ensemble average) (isotropic motion)	-14%	-13%	-10%	-21%	-29%	-12%
CALCULATED (Ido A rings in 0S2) (symmetric top)	-6%	-15%	-2%	-22%	-13%	-3%
CALCULATED (Ido A rings in 0S2) (isotropic motion)	-14%	-16%	-5%	-30%	-21%	-9%

*No stereospecific assignment was performed . ‡ensemble average and symmetric top model.